Heliyon 10 (2024) e24257

Contents lists available at ScienceDirect

Heliyon

journal homepage: www.cell.com/heliyon

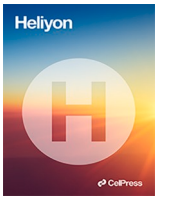

Research article

Application of synchronized tandem welding to high-hardness armor steel

Bo Wook Seo [a], Young Cheol Jeong [b], Hwi Jun Son [a], Chang Jong Kim [a], Seok Kim [a,c], Young Tae Cho [a,c,*]

[a] Department of Smart Manufacturing Engineering, Changwon National University, 20, Changwondaehak-ro, Uichang-gu, Changwon-si, Gyeongsangnam-do, 641-241, Republic of Korea
[b] Korea Textile Machinery Convergence Research Institute, 27, Sampung-ro, Gyeongsan-si, Gyeongsangbuk-do, 38542, Republic of Korea
[c] Department of Mechanical Engineering, Changwon National University, 20, Changwondaehak-ro, Uichang-gu, Changwon-si, Gyeongsangnam-do, 641-241, Republic of Korea

ARTICLE INFO

Keywords:
Tandem gas metal arc welding
Mechanical property
High-hardness-armor steel
Weldability

ABSTRACT

Several studies have been conducted to improve combat vehicle capabilities, such as the bullet-proof performance of armor and fuel efficiency through weight reduction. Titanium alloys and ceramic materials are expensive and difficult to process; therefore, they can be applied only in specific locations. In addition, arc welding, which is relatively inexpensive compared with other welding processes, is widely used in industrial fields; however, because welding is often performed in multiple passes to join one part, the productivity is reduced. Therefore, in this study, mechanical properties were investigated according to production time and heat input by applying tandem pulse gas metal arc welding (GMAW) to increase productivity. The experimental data were obtained by varying the wire feeding speed. In addition, the current–voltage waveforms were measured, and the volume shift was analyzed by comparison with images captured using a high-speed camera. To analyze the mechanical properties of the tandem weld for the welding of high-hardness armor plates, the appearance (top bead and back bead), cross-section, hardness, tensile test, impact test, and spatter generation of the welded part were analyzed. The results show that all Tank-automotive and Armaments Command (TACOM) standards for the base material were met when the tandem wire feeding speed was 11 + 11 m/min, and the single-pass process increased production speed by a factor of more than 10. Tandem pulse GMAW is shown to be a viable option for improving productivity and maintaining high-quality welds for high-hardness materials.

1. Introduction

Recently, in the defense industry, research and development for weight reduction of materials has been actively conducted, and in the case of combat vehicles, much research is being conducted on weight reduction of armor plates [1,2]. Although armor plate performance is the most important indicator of occupant safety, heavy weight causes the problem of low mobility. Consequently,

* Corresponding author. Department of Smart Manufacturing Engineering, Changwon National University, 20, Changwondaehak-ro, Uichang-gu, Changwon-si, Gyeongsangnam-do, 641-241, Republic of Korea.
E-mail address: ytcho@changwon.ac.kr (Y.T. Cho).

https://doi.org/10.1016/j.heliyon.2024.e24257
Received 28 August 2023; Received in revised form 13 November 2023; Accepted 5 January 2024
Available online 6 January 2024

combat capability is reduced owing to the reduced range of movement, restriction of military transfer, and increased fuel consumption. To solve this problem, many studies have been conducted to reduce weight by reducing plate thickness or producing a porous [3] or lattice structure [4] while maintaining bulletproof performance. Various armor materials, such as titanium and steel [5], are being developed for weight reduction, and titanium alloys [6] and ceramic materials [7] are being applied as non-ferrous armor materials. Titanium alloys and ceramic materials are used only in limited areas because of their high cost and difficult welding [8] and processing characteristics. In contrast, high-hardness armor (HHA) [9], rolled homogeneous armor (RHA) [10], and ultra-high-hardness armor (UHA) [11] steels, which are inexpensive and exhibit excellent strength, workability, and weldability, are widely used.

Among these, HHA steel presents various challenges due to its high carbon content [12]. The primary issue with high-carbon steels is that instead of forming tempered martensite with high hardness in the heat-affected zone (HAZ), they become brittle [13]. Furthermore, there's a heightened likelihood of cold cracking [14], necessitating an evaluation of weldability. Numerous studies have been undertaken to mitigate the risk of cold cracks during the welding of HHA steel [15]. Low-hydrogen ferritic (LHF) steel consumables, which don't contain hygroscopic compounds, are employed for welding HHA steel [16]. Vasconcelos et al. [17] introduced a welding technique that incorporates cold wire during the welding of HHA plates, aiming to enhance the microstructure.

In addition to research on materials, various studies have been conducted on welding processes. Typically, the welding processes used to join HHA plates include laser [18], submerged arc welding (SAW) [19], gas metal arc welding (GMAW) [20], gas tungsten arc welding (GTAW) [21], shielded metal arc welding (SMAW), and flux-cored arc welding (FCAW) [22]. Magudeeswaran et al. [22] investigated and evaluated the degree of hydrogen-induced cracking (HIC) according to the welding process using SMAW and FCAW. Bassett [23] welded HHA plates with laser and evaluated the size and hardness of the HAZ, Charpy toughness, and ballistic behavior. In addition, Son et al. [20] evaluated the weldability of HHA steel according to US Army standards, such as impact performance, tensile strength, and HAZ size, using GMAW.

While many welding processes are amenable to automation, automating the welding of large structures remains challenging. Productivity might suffer due to the thermal deformation of materials and the necessity of multiple passes [24,25]. To enhance deposition rates and welding speed in conventional welding processes, numerous studies have explored the benefits of tandem welding, which employs two arc heat sources. For welding a V-groove shape with standard GMAW, a multi-pass welding method is typically used. In contrast, tandem welding can achieve the desired bead width and penetration depth in a single pass [26]. Additionally, significant research aims to boost productivity by introducing extra filler metals [27]. In the context of HHA plates, the strength of the HAZ can diminish due to elevated heat input, necessitating a thorough analysis [28]. Given that arc interactions transpire between the dual heat sources, research has predominantly centered on understanding the dynamics of the molten pool [29]. It's essential to assess weld defects and strength by examining the HAZ's robustness and the molten pool's behavior influenced by arc interactions. In this study, we applied tandem welding to bond HHA plates and evaluated the resulting weldability.

2. Experiment equipment and methods

The experiment was conducted using a Fronius TPS 5000 welding machine and an industrial ABB robot. For welding, V-groove specimens with dimensions of 250 mm × 500 mm and a thickness of 12 mm were prepared, and their weldability was evaluated. Additionally, all welding specimens were preheated to 150° using a torch before performing the test. The experimental setup is shown in Fig. 1. Tandem welding was performed using two synchronized power sources. The current and voltage data were captured using the

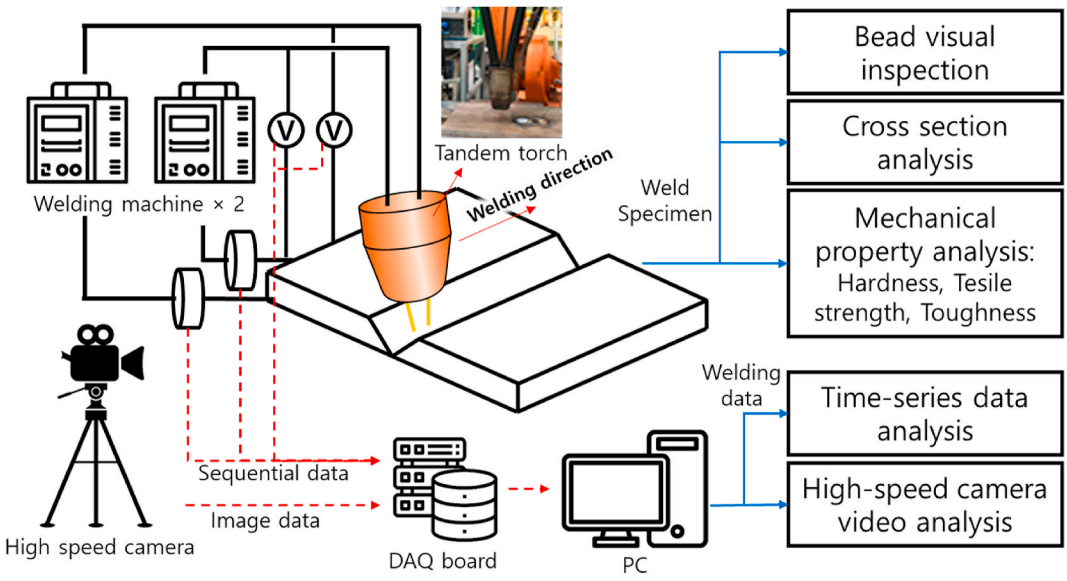

Fig. 1. Schematic of data measurement and specimen analysis in a tandem welding system.

data acquisition (DAQ) board and then processed and analyzed on a PC. Separately, images of the molten pool dynamics were obtained using a high-speed camera. In addition, the characteristics of the welded parts according to the welding conditions were confirmed through photographs and mechanical property analyses. The tank-automotive and armaments command (TACOM) standard was used as a criterion for evaluating weldability [30].

For the welding conditions, the same mechanical strength was confirmed by changing the wire feeding speed (WFS) on the basis of the optimal heat input conditions determined for single-pulse GMAW. Table 1 lists the welding conditions used in this study. The experiment utilized a domestic HHA plate, with a Vickers hardness ranging from 460 to 510 HV and a tensile strength between 1600 and 1700 MPa, as shown in Tables 2 and 3. The wire used for welding was ER120S-G with a tensile strength of 830 MPa and an elongation of 12 %. Table 4 lists the chemical composition ratios of the welding wire.

3. Results and discussion

3.1. Weld visual inspection

After performing tandem welding while controlling the welding wire supply speed, the appearance quality was visually inspected. Fig. 2 shows a photograph illustrating the variations in the top bead and back bead as influenced by WFS. When the WFS was 9 m/min for both torches, no back bead was formed. When the WFS was 11 m/min, no back bead was formed; however, this condition did not affect the weld quality. As the WFS increased, the penetration depth increased, and weld back bead formation occurred smoothly.

3.2. Tandem process current–voltage waveform and volume transfer analysis

The droplet transfer and process stability according to welding WFS were identified using high-speed camera images and welding current–voltage waveforms. Fig. 3 shows the current and voltage changes occurring during tandem welding. As two power sources were used for synchronized tandem welding, the current of the leading and trailing torches increased alternately. Furthermore, the current of the leading torch exhibits a higher value than that of the trailing torch. As the wire of the leading torch melts, the molten pool rises, causing the stick out of the trailing torch to decrease, leading to an increase in its current. The molten pool generated by the leading torch can alter the voltage of the trailing torch. When the wire of the trailing torch comes into contact with the wire of the leading torch, a short circuit occurs, causing the voltage to converge to zero. At this moment, to disconnect the wire, an excessive voltage is applied from the welding power source, allowing the maintenance of the arc plasma. This phenomenon enables continuous welding. However, at 9 m/min, despite the smallest amount of metal being melted, a large number of short circuits occur. This is because the mechanism of metal transfer changes depending on the current value. In this condition, short circuits occur frequently, while in other conditions, the transition to spray mode reduces the occurrence of short circuits. This can be observed in the high-speed camera images in Fig. 4. Taking all these factors into account, we can conclude that the most stable welding occurs at 11 m/min. As previously mentioned, the flow of the molten pool can lead to arc instability. Additionally, the magnetic forces generated between the two wires and the base material, as well as arc interference caused by the arc itself, can further contribute to arc instability.

The high-speed image in Fig. 4 shows that as the welding WFS increased, the welding magnetic blow increased and arc interactions occurred frequently. This phenomenon occurred because the pulse current period decreased as the current increased. The high-speed camera image shows that the volume transfer at 9 + 9 m/min was more stable than that at 11 + 11 m/min. However, under the condition of 9 + 9 m/min, it was difficult to apply because the penetration was insufficient.

3.3. Weld section analysis

As shown in the cross-sectional analysis of the weld section in Fig. 5, no pores or cracks were observed in the tandem weld section. It was confirmed that the penetration increased as the WFS increased, as in the external bead test result. In addition, the welding part, which required multiple passes in general pulse GMAW, was formed in only one pass.

3.4. Hardness analysis result

A Vickers hardness test was performed and the hardness profile was confirmed using HV1. The hardness was measured at intervals of 1 mm. Fig. 6 shows the welding hardness distribution results according to the welding WFS conditions. The hardness of the weld

Table 1
Welding conditions for the nano particle flux experiment.

Welding process	Tandem GMAW		
Welding speed (cm/min)	30		
Shielding gas	Ar + CO_2 10 %		
Joint	V-groove		
Wire feeding speed (WFS) (m/min)	9	11	13
Contact tip with distance (CTWD) (mm)	20		
Number of passes	1		

Table 2
Chemical properties of HHA steel (wt%).

Fe	C	Mn	Si	Ni	Mo	Cr	Al	V	Ti	CEQ
Bal.	0.27	0.96	0.22	3.04	0.29	0.49	0.09	0.03	0.02	0.69

Table 3
Mechanical properties of HHA steel.

Hardness (HV)	Charpy-V (J)	Yield Strength (MPa)	Tensile Strength (MPa)	Elongation A5 (%)
460–510	29	1357	1672	Longitudinal: 17 Transverse: 14

Table 4
Chemical properties of welding wire (ER120S-G) (wt%).

Fe	C	Mn	Si	Ni	Mo	S	P
Bal.	0.06	1.48	0.003	3.42	0.57	0.003	0.002

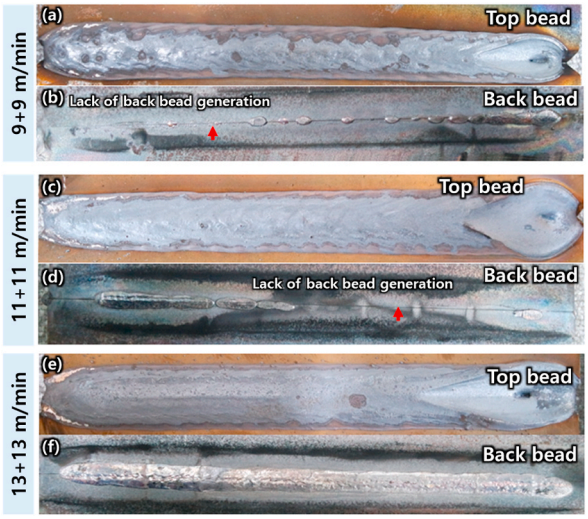

Fig. 2. Images illustrating the variations in tandem welding beads influenced by wire feeding speed (WFS) under the following conditions: (a) and (b) 9 + 9 m/min; (c) and (d) 11 + 11 m/min; (e) and (f) 13 + 13 m/min (a), (c), (e) show the top bead; (b), (d), (f) depict the back bead.

metals was lower than that of the base material. It was confirmed that the hardness of the HAZ part was higher than that of the weld metal under all conditions. Furthermore, as shown in Fig. 5, the HAZ expanded as the amount of heat input increased. As shown in Fig. 6, the hardness distribution within the HAZ varies with the changing width of the Heat-Affected Zone due to different WFS conditions. Notably, when the speed is at 9 + 9 m/min, the hardness of the HAZ appears to be higher. This is attributed to the characteristic of high-hardness steel, where the hardness decreases as the heat input increases [31].

3.5. Tensile test results

Tensile tests were conducted according to the TACOM standard at a test speed of 3 mm/min. The tensile test results are shown in Fig. 7. The tensile strength of the weld under all WFS conditions exceeded that of the ER120S-G welding wire. In addition, similar to the hardness results of the tandem welds, there was no significant change in the tensile strength, even when the WFS conditions were changed. However, elongation tended to decrease under faster WFS conditions. The elongation of the weld was confirmed to be lower than that of the wire.

3.6. Impact test results

For impact testing, the Charpy test was conducted at −40 °C. Specimen production and testing were evaluated in compliance with

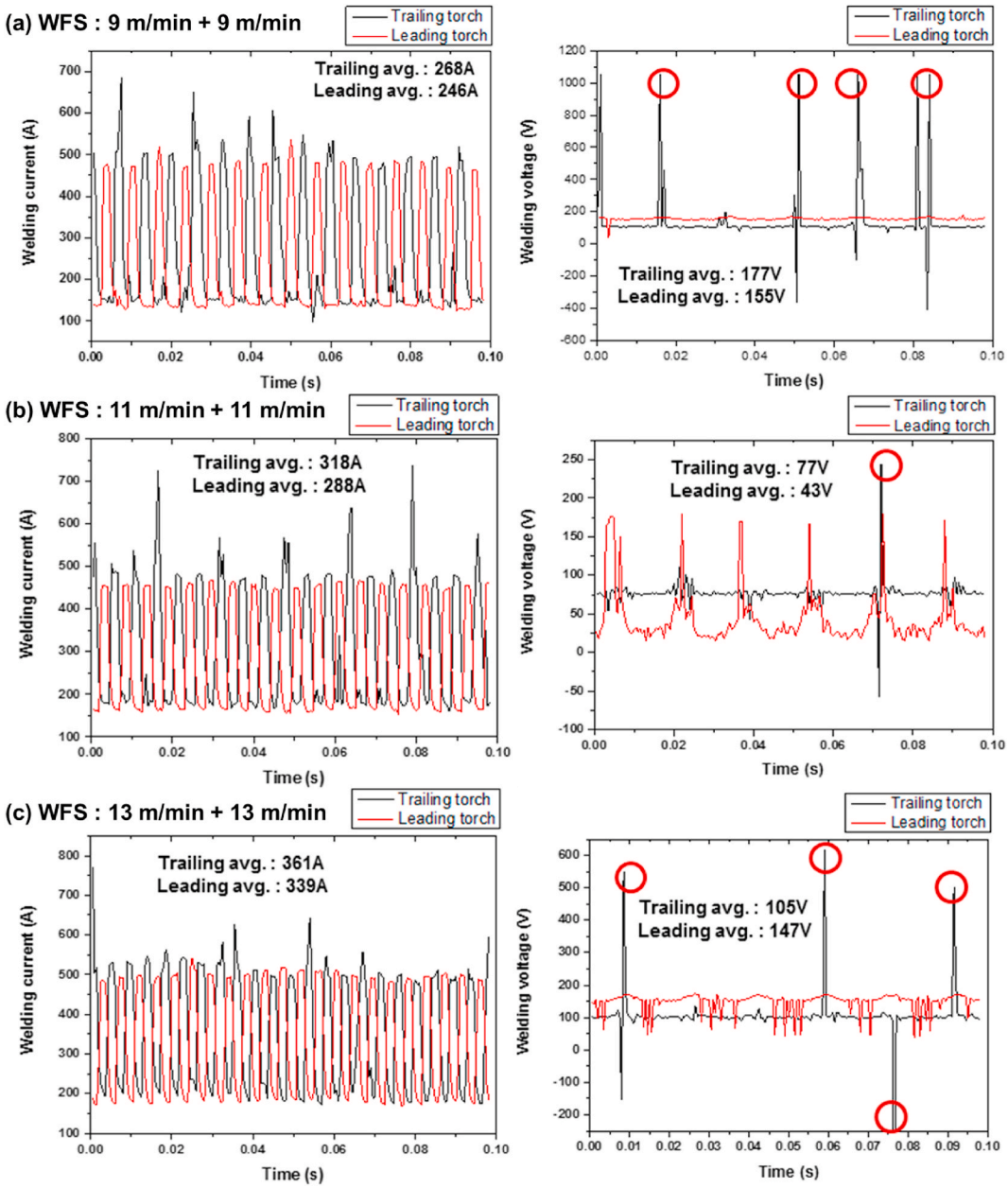

Fig. 3. Current and voltage waveform change in tandem welding with WFS conditions (a) 9 + 9 m/min, (b) 11 + 11 m/min, and (c) 13 + 13 m/min.

the American Society for Testing and Materials (ASTM) standards. The low-temperature impact characteristics of the tandem weld and hardened area were tested, and the low-temperature impact results were confirmed, as shown in Fig. 8. Low-temperature impact characteristics greater than 16.4 J, which is the TACOM standard for high-hardness armored materials, were confirmed under all supply speed conditions. The highest low-temperature impact characteristics were confirmed at a WFS of 9 m/min. As the WFS increased, the low-temperature impact properties decreased.

3.7. Spatter generation analysis

Spatter analysis was conducted using images from the tandem pulse GMAW process. As depicted in Fig. 9, we acquired images of the welded specimen and calculated the spatter quantity in pixels through image preprocessing. The tandem pulse GMAW at WFS of 9 + 9 m/min and 11 + 11 m/min produced less spatter compared to general-pulse GMAW. However, at a WFS of 13 + 13 m/min, a notably larger amount of welding spatter was evident, as observed in the tandem welding process current–voltage waveform and high-speed camera images.

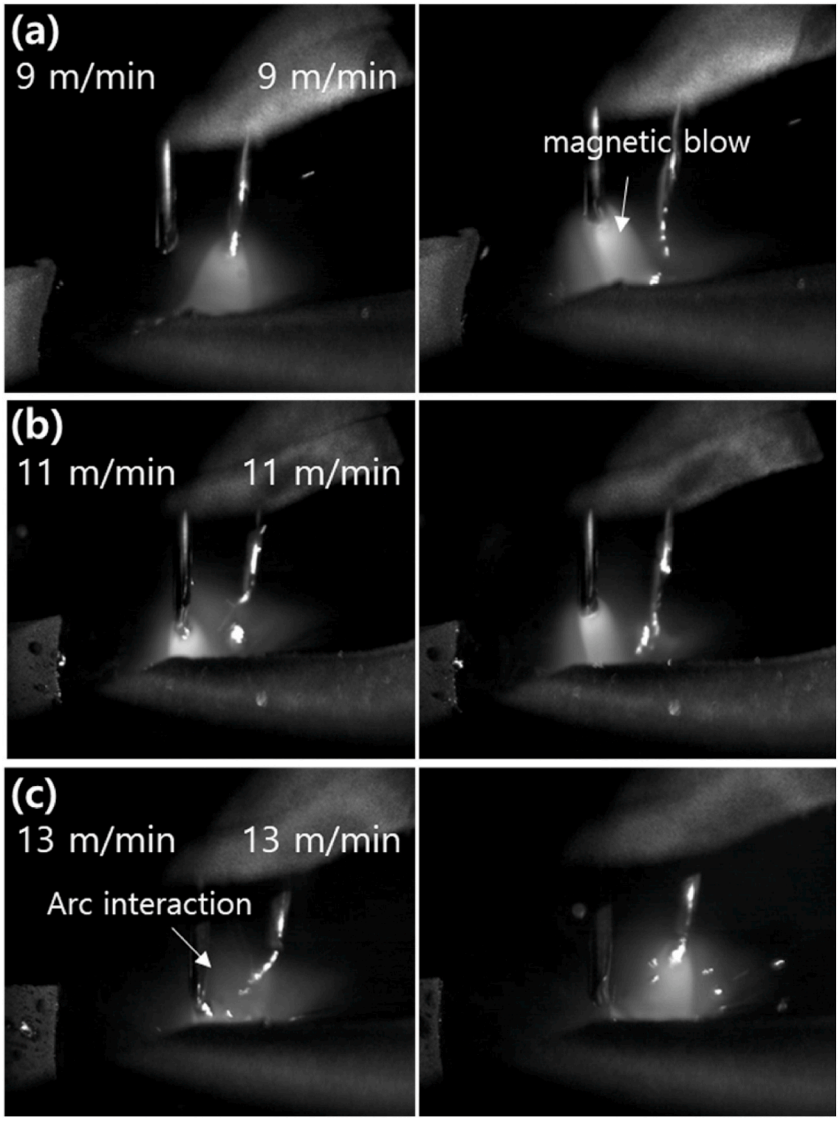

Fig. 4. High-speed image of tandem metal transfer and arc interaction. WFS: (a) 9 + 9 m/min, (b) 11 + 11 m/min, (c) 13 + 13 m/min.

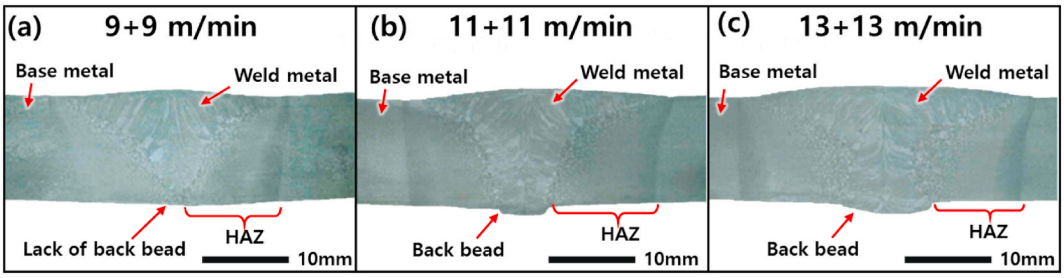

Fig. 5. Comparison of cross-sectional views in tandem pulse GMAW: (a) 9 + 9 m/min, (b) 11 + 11 m/min, (c) 13 + 13 m/min.

4. Conclusion

In this study, the potential of tandem pulse GMAW to enhance productivity without compromising weld quality for high-hardness materials was explored. Utilizing an automated system with a welding robot, tandem welding was executed with precision, and a

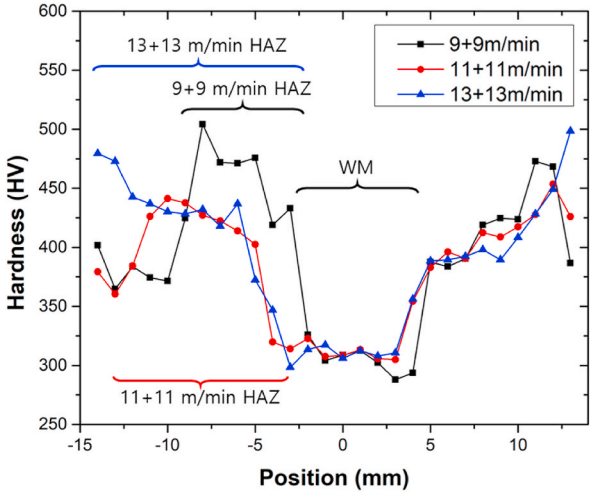

Fig. 6. Hardness profile in tandem welding process at different WFS conditions.

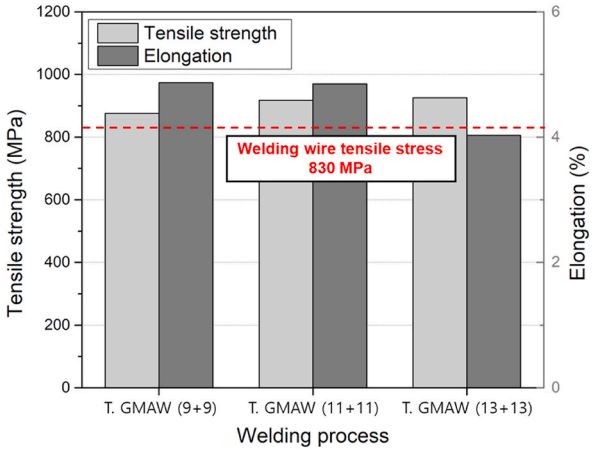

Fig. 7. Comparison graph of tensile strength and elongation results in single and tandem welding processes.

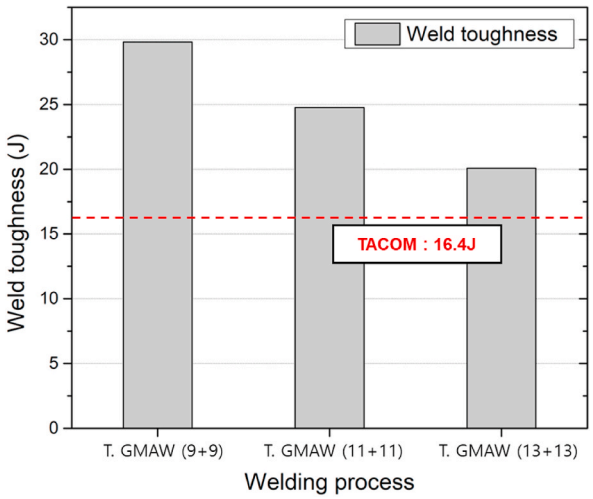

Fig. 8. Comparison graph of −40 °C toughness results in welds of the single and tandem welding processes.

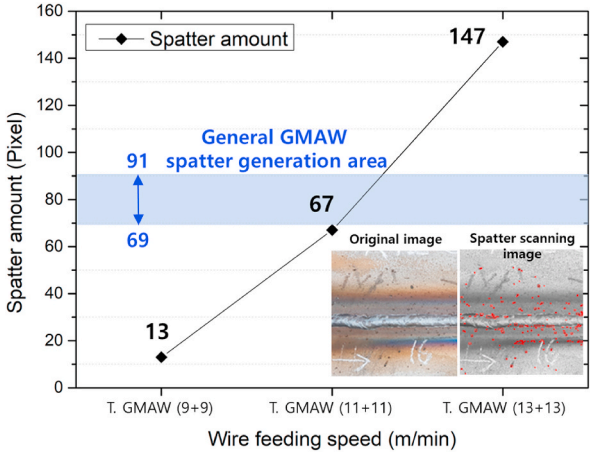

Fig. 9. Amount of welding spatter generation in the tandem welding process.

dedicated current and voltage measurement system was set up to ensure process stability.

Mechanical tests on V-groove specimens, with synchronized WFS for both leading and trailing torches, were pivotal in assessing the weldability of tandem GMAW. Our observations revealed that a WFS of 11 + 11 m/min yielded the most consistent results in terms of current and voltage stability, ensuring complete back bead formation. While larger heat inputs expanded the HAZ and reduced hardness, the tensile strength peaked at the aforementioned WFS. However, as the WFS increased to 13 + 13 m/min, there was a noticeable decline in elongation and low-temperature impact strength, coupled with a rise in spatter generation.

Crucially, the tandem GMAW approach met all TACOM standards for the base material at a WFS of 11 + 11 m/min. This method has the potential to transform the traditional multi-pass welding process into a more efficient single-pass procedure, amplifying production speed considerably.

In summary, tandem pulse GMAW emerges as a promising technique for high-hardness materials, offering both enhanced productivity and superior weld quality. The insights gained from this study lay the groundwork for refining welding conditions in subsequent investigations.

Funding statement

This result was supported by the National Research Foundation of Korea (NRF) grant funded by the Korea government (MSIT) (No. 2019R1A5A8083201) and supported by “Regional Innovation Strategy (RIS)” through the National Research Foundation of Korea (NRF) funded by the Ministry of Education (MOE) (2021RIS-003).

Data availability statement

Data will be made available on request.

Additional information

No additional information is available for this paper.

CRediT authorship contribution statement

Bo Wook Seo: Writing - review & editing, Writing - original draft, Visualization, Validation, Software, Resources, Methodology, Formal analysis, Data curation, Conceptualization. **Young Cheol Jeong:** Writing - original draft, Visualization, Validation, Project administration, Methodology, Investigation, Formal analysis, Data curation, Conceptualization. **Hwi Jun Son:** Project administration, Formal analysis, Data curation. **Chang Jong Kim:** Validation, Supervision, Software, Investigation. **Seok Kim:** Writing - review & editing, Writing - original draft, Supervision, Methodology, Conceptualization. **Young Tae Cho:** Writing - review & editing, Writing - original draft, Validation, Supervision, Resources, Project administration, Methodology, Funding acquisition, Formal analysis, Conceptualization.

Declaration of competing interest

The authors declare that they have no known competing financial interests or personal relationships that could have appeared to influence the work reported in this paper.

References

[1] S. Abdullah, M.F. Abdullah, W.M. Jamil, Ballistic performance of the steel-aluminium metal laminate panel for armoured vehicle, J. Mech. Eng. Sci. 14 (1) (2020) 6452–6460, https://doi.org/10.15282/jmes.14.1.2020.20.0505.

[2] Y. Guo, J.H. Wang, X.Y. Xu, T.T. Duan, et al., Ballistic performance of protection structures using fiber composites as matrix armor, J. Phys. Conf. Ser. 2460 (1) (2023) 012126, https://doi.org/10.1088/1742-6596/2460/1/012126.

[3] F.J. Ramírez-Gil, E.C.N. Silva, W. Montealegre-Rubio, Through-thickness perforated steel plates optimized for ballistic impact applications, Mater. Des. 212 (2021) 110257, https://doi.org/10.1016/j.matdes.2021.110257.

[4] A. Jinnapat, P. Doungkom, K. Somton, K. Dateraksa, Ballistic performance of composite armor impacted by 7.62 mm armor projectile, J. Met. Mater. Miner. 33 (2) (2023) 120–127, https://doi.org/10.55713/jmmm.v33i2.1698.

[5] T. Fu, M. Zhang, Q. Zheng, D. Zhou, X. Sun, X. Wang, Scaling the response of armor steel subjected to blast loading, Int. J. Impact Eng. 153 (2021) 103863, https://doi.org/10.1016/j.ijimpeng.2021.103863.

[6] P. Li, Q. Fan, X. Zhu, H. Gong, Study of high-speed-impact-induced conoidal fracture of Ti alloy layer in composite armor plate composed of Ti-and Al-alloy layers, Def. Technol. 17 (4) (2021) 1434–1443, https://doi.org/10.1016/j.dt.2020.07.010.

[7] Y.X. Zhai, H. Wu, Q. Fang, Impact resistance of armor steel/ceramic/UHPC layered composite targets against 30CrMnSiNi2A steel projectiles, Int. J. Impact Eng. 154 (2021) 103888, https://doi.org/10.1016/j.ijimpeng.2021.103888.

[8] B.K. Nagesha, V. Dhinakaran, M. Varsha Shree, K.P. Manoj Kumar, T. Jagadeesha, A review on weldability of additive manufactured titanium alloys, Mater. Today: Proc. 33 (2020) 2964–2969, https://doi.org/10.1016/j.matpr.2020.02.899.

[9] M.C. Jo, S. Kim, D.W. Kim, H.K. Park, et al., Understanding of adiabatic shear band evolution during high-strain-rate deformation in high-strength armor steel, J. Alloys Compd. 845 (2020) 155540, https://doi.org/10.1016/j.jallcom.2020.155540.

[10] P. Yin, C. Xu, Q. Pan, W. Zhang, X. Jiang, Effect of different ultrasonic power on the properties of RHA steel welded joints, Mater 15 (3) (2022) 768, https://doi.org/10.3390/ma15030768.

[11] N.K. Subramani, B. Visvalingam, M. Sudersanan, H.R. Abdur, B. Vadivel, Influence of welding consumables on ballistic performance of gas metal arc welded ultra-high hard armor steel joints, Mater. Perform. Charact. 10 (1) (2021) 443–462, https://doi.org/10.1520/MPC20200150.

[12] Z. Fei, Z. Pan, D. Cuiuri, H. Li, A.A. Gazder, A combination of keyhole GTAW with a trapezoidal interlayer: a new insight into armour steel welding, Mater 12 (21) (2019) 3571, https://doi.org/10.3390/ma12213571.

[13] A. Cabrilo, K. Geric, Weldability of high hardness armor steel, Adv. Mater. Res. 1138 (2016) 79–84. https://doi.org/10.4028/www.scientific.net/AMR.1138.79.

[14] S.J. Alkemade, The Weld Cracking Susceptibility of High Hardness Armour Steel, DSTO Aeronautical and Maritime Research Laboratory, 1996, pp. 1–27.

[15] G. Magudeeswaran, V. Balasubramanian, G.M. Reddy, Hydrogen induced cold cracking studies on armour grade high strength, quenched and tempered steel weldments, Int. J. Hydrog. Energy 33 (7) (2008) 1897–1908, https://doi.org/10.1016/j.ijhydene.2008.01.035.

[16] G. Magudeeswaran, V. Balasubramanian, G.M. Reddy, T.S. Balasubramanian, Effect of welding processes and consumables on tensile and impact properties of high strength quenched and tempered steel joints, J. Iron Steel Res. Int. 15 (6) (2008) 87–94, https://doi.org/10.1016/S1006-706X(08)60273-3.

[17] C.H. Vasconcelos, C. Loayza, P.D. Assunção, F.F. Junior, et al., High-hardness armor welded by CW-GMAW: economic, geometric and CGHAZ analysis, J. Braz. Soc. Mech. Sci. Eng. 41 (2019) 1–11, https://doi.org/10.1007/s40430-019-1756-1.

[18] D. Janicki, Disk laser welding of armor steel/spawanie laserem dyskowym stali pancernej, Arch. Metall. Mater. 59 (2014), https://doi.org/10.2478/amm-2014-0279.

[19] S. Taskaya, A.K. Gur, C. Ozay, Joining of Ramor 500 steel with SAW (submerged Arc welding) and its evaluation of thermomechanical analysis in ANSYS package software, Therm. Sci. Eng. Prog. 13 (2019) 100396, https://doi.org/10.1016/j.tsep.2019.100396.

[20] H.J. Son, Y.C. Jeong, B.W. Seo, S. Hong, Y. Kim, Y.T. Cho, Weld quality analysis of high-hardness armored steel in pulsed gas metal arc welding, Metals 13 (2) (2023) 303, https://doi.org/10.3390/met13020303.

[21] G.M. Reddy, T. Mohandas, K.K. Papukutty, Effect of welding process on the ballistic performance of high-strength low-alloy steel weldments, J. Mater. Process. Technol. 74 (1–3) (1998) 27–35, https://doi.org/10.1016/S0924-0136(97)00245-8.

[22] G. Magudeeswaran, V. Balasubramanian, G.M. Reddy, Effect of welding processes and consumables on high cycle fatigue life of high strength, quenched and tempered steel joints, Mater. Des. 29 (9) (2008) 1821–1827, https://doi.org/10.1016/j.matdes.2008.03.006.

[23] J. Bassett, Laser welding of high hardness armour steel, Sci. Technol. Weld. Join. 3 (5) (1998) 244–248, https://doi.org/10.1179/stw.1998.3.5.244.

[24] B.W. Seo, D. Kim, C. Kim, S. Kim, Y.T. Cho, Development of seam tracking device in asynchronous tandem welding with arc sensing, Sci. Rep. 12 (1) (2022) 18637, https://doi.org/10.1038/s41598-022-23299-2.

[25] B.W. Seo, Y.C. Jeong, Y.T. Cho, Machine learning for prediction of arc length for seam tracking in tandem welding, J. Weld. Join. 38 (3) (2020) 241–247, https://doi.org/10.5781/JWJ.2020.38.3.2.

[26] L.F.S. Rossini, R.A.V. Reyes, J.E. Spinelli, Double-wire tandem GMAW welding process of HSLA50 steel, J. Manuf. Process. 45 (2019) 227–233, https://doi.org/10.1016/j.jmapro.2019.07.004.

[27] J. Kim, J. Park, J. Jang, S.H. Lee, Control of droplet transfer using a filler-wire in tandem arc welding, Sci. Technol. Weld. Join. 26 (2) (2021) 123–129, https://doi.org/10.1080/13621718.2020.1848979.

[28] A.K. Pramanick, H. Das, G.M. Reddy, M. Ghosh, et al., Development and design of microstructure based coated electrode for ballistic performance of shielded metal arc welded armour steel joints, Mater. Des. 103 (2016) 52–62, https://doi.org/10.1016/j.matdes.2016.04.058.

[29] G. Liu, S. Han, X. Tang, H. Cui, Effects of torch configuration on arc interaction behaviors and weld defect formation mechanism in tandem pulsed GMAW, J. Manuf. Process. 62 (2021) 729–742, https://doi.org/10.1016/j.jmapro.2021.01.007.

[30] US Department of Defense, MIL-A-12560h—Armor Plate, Steel, Wrought, Homogeneous, 1990.

[31] B. Savic, A. Cabrilo, Effect of heat input on the ballistic performance of armor steel weldments, Materials 14 (13) (2021) 3617, https://doi.org/10.3390/ma14133617.